NANO LETTERS

pubs.acs.org/NanoLett Letter

Strain-Correlated Piezoelectricity in Quasi-Two-Dimensional Zinc Oxide Nanosheets

Corey Carlos, Jun Li, Ziyi Zhang, Kevin Jordan Berg, Yizhan Wang, and Xudong Wang*

Cite This: https://doi.org/10.1021/acs.nanolett.3c01728 Read Online

ACCESS | Metrics & More | Article Recommendations | Supporting Information

ABSTRACT: Two-dimensional (2D) piezoelectric materials have recently drawn intense interest in studying the nanoscale electromechanical coupling phenomenon and device development. A critical knowledge gap exists to correlate the nanoscale piezoelectric property with the static strains often found in 2D materials. Here, we present a study of the out-of-plane piezoelectric property of nanometer-thick 2D ZnO-nanosheets (NS) in correlation to in-plane strains, using *in situ* via strain-correlated piezoresponse force microscopy (PFM). We show that the strain configuration (either tensile or compressive) can dramatically influence the measured piezoelectric coefficient (d_{33}) of 2D ZnO-NS. A comparison of the out-of-plane piezoresponse is made for in-plane tensile and compressive strains approaching 0.50%, where the measured d_{33} varies between 2.1 and 20.3 pm V^{-1} resulting in an order-of-magnitude change in the piezoelectric property. These results highlight the important role of in-plane strain in the quantification and application of 2D piezoelectric materials.

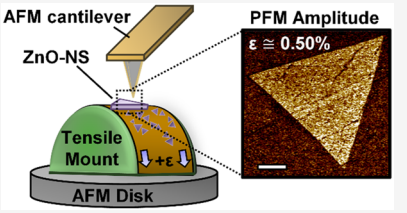

KEYWORDS: *2D nanomaterials, nanoscale piezoelectricity, PFM, strain coupling, ZnO*

Strain engineering has long been utilized to enhance the mechanical and physical properties of functional electronic and photonic devices, where coupling between material properties has enhanced the field of wearable electronics, intelligent sensing, energy harvesting, and biointegration.[1−9] Studying the strain-related property change has shown substantial significance in 2D materials developments. For example, polymer encapsulation and surface modification are effective techniques for transferring uniaxial strain into 2D transition metal dichalcogenides (TMD), where enhanced optical properties were achieved by strain induced bandgap modulation.[3,9] Microheater actuators were used for inducing up to 0.64% biaxial strain in single-layered MoS_2 by controlling the thermal expansion in the supporting substrate.[4] Utilizing the mechanical stimuli of biological movement and ambient vibrations to actively modulate the electronic functionality of wearable devices, the broadening field of piezotronics has effectively harnessed the piezoelectric properties enhanced by (or evolved from) two-dimensional (2D) materials (such as ZnO, MoS_2, GaN, etc.) for next-generation flexible electronics.[10−12] Since the heterogeneous components that comprise flexible devices can induce sufficiently large in-plane strains, an in-depth understanding of the strain-related piezoelectric behavior is critical for advancing the seamless integration of electronic properties with mechanical actuations. Yet, there remains a critical knowledge gap regarding the piezoelectric property of 2D materials incorporated into heterogeneous device schemes when subjected to large in-plane strain. Because of this gap, our capability to accurately predict or analyze the piezoelectric performance of 2D electromechanical devices is rather limited. Current understandings of the nanoscale piezoelectric property are either directly leveraged from bulk materials or determined from unstrained or relaxed lattice configurations.

Zinc oxide (ZnO) has shown to be an excellent candidate for exploring the coupling effects between piezoelectric and semiconducting properties, known as piezotronics.[13−18] ZnO-based piezotronic device schemes typically utilize the dominant piezoelectric coefficient (d_{33} [pm V^{-1}]) oriented along the [0001] direction of wurtzite ZnO (*c*-axis), harnessing the piezoelectric surface charge to control electronic transport. Recently, 2D ZnO nanosheets (ZnO-NSs) synthesized via ionic layer epitaxy (ILE),[19−21] with thickness ranging between 1−4 nm, have illustrated strong out-of-plane d_{33} values as high as 18.9 pm V^{-1}, nearly doubling their bulk ZnO counterpart.[22] Given the large degree of thickness control[21,23] and high d_{33} value, ILE ZnO-NSs offer a promising platform for exploring the stress−strain relationship with the linear electromechanical coupling of the piezoelectric property in the nanometer regime. Furthermore, the large surface-to-volume ratio of ZnO-NSs offers a unique opportunity to uncover the contribution of in-plane piezoelectric tensors on traditional *c*-axis device schemes. Here, we address the in-plane strain contributions on the out-of-plane piezoelectric property of [0001] ZnO-NSs, by introducing *in situ* strain-correlated piezoresponse force microscopy (PFM). The piezoelectric coefficients are extracted

Received: May 9, 2023
Revised: June 25, 2023

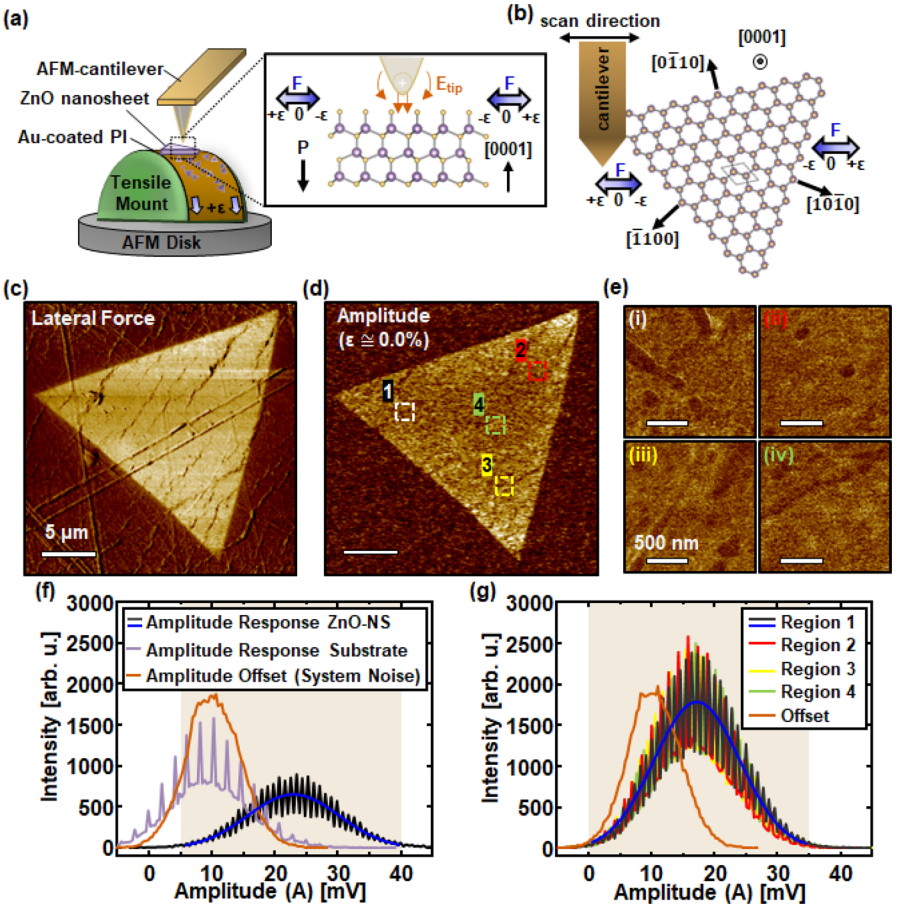

Figure 1. Characterization of the piezoelectric property of a ZnO-NS under uniaxial strain. (a) Schematic of testing setup of strain-correlated PFM on ZnO-NSs. Inset illustrates the relationship between electric field, applied strain and the [0001] direction of wurtzite ZnO. (b) Schematic of the PFM scan across the (0001) plane and the strain direction relationship. (c) Lateral force microscopy (LFM) showing a ZnO-NS supported on a Au-coated PI substrate. (d) Typical large scan area PFM amplitude image of a ZnO-NS without any strain. (e) Four small scan area PFM amplitude images taken from the ZnO-NS surface as indicated in (d). (f, g) Image intensities extracted as functions of amplitude responses of the ZnO-NS from the large (f) and small (g) scan areas.

for a series of compressive and tensile strain configurations of ILE grown ZnO-NSs. This research uncovers how the d_{33} of a 2D piezoelectric material may be coupled to in-plane strains at the nanometer scale, offering insights into additional coupling effects for flexible piezoelectric nanodevice design.

Figure 1 shows a schematic of a strain-correlated PFM experiment used to examine the nanoscale piezoelectric property of ZnO-NSs. Application of in-plane strain was achieved using a series of 3D printed mounts, which enabled different convex and concave bending configurations (see Supplemental Figure S1) to the flexible sample substrates (tensile configuration shown in Figure 1a). As-synthesized ZnO-NSs were transferred onto a flexible Au-coated polyimide (PI) substrate, which was affixed to a curved mount to provide constant strain during the PFM scan. Strong adhesion between the ZnO-NSs and Au-coated PI substrate, along with a nominal Young's modulus of the PI ($E_{Young} \sim 2.1$ GPa)[24] ensured an efficient strain transfer between substrate and the ZnO-NSs. Because the thickness of the ZnO-NSs was orders of magnitude smaller than that of the PI substrate, we could assume applied strain ($\pm\varepsilon$) to be uniaxial for both tensile ($+\varepsilon$) and compressive ($-\varepsilon$) strain configurations. Application of the static uniaxial strain was determined to be normal to the [0001] axis and across the basal plane of the wurtzite ZnO-NS (illustrated in Figure 1b).[25]

Given the extremely thin thickness of the NSs (typically $t <$ 5 nm), along with relatively large surface roughness ($Ra \sim 3.4$ nm) and imperfections on the flexible PI substrate, typical topography scans could not accurately characterize the ZnO-NS thickness or morphology. To determine the thickness, ZnO-NSs synthesized under the same conditions were transferred onto rigid and flat Au-coated Si substrates (nominal $Ra \sim 0.4$ nm), which revealed the NSs had a fairly uniform thickness of $t \sim 2.4$ nm (Supplemental Figure S3).

However, the need remained to exactly characterize the location and morphology of the target ZnO-NS on a flexible PI-substrate for accurate strain-correlated PFM characterization. A lateral force microscopy (LFM) method was employed to strictly resolve the location and morphology of ZnO-NS shown in Figure 1c. LFM is a contact mode AFM measurement which utilizes the lateral forces associated with changes of frictional coefficients at the tip−sample interface as the probe raster scans across a sample surface.[26,27] Since the probe dynamics that govern PFM measurements occur in the same contact regime, this coupled LFM/PFM technique offered a unique solution to characterize low-dimensional materials on substrates with large surface roughness but inhomogeneous surface friction.

During each strain-correlated PFM measurement, the AFM probe slowly approached the ZnO-NS surface until tip−sample

https://doi.org/10.1021/acs.nanolett.3c01728
Nano Lett. XXXX, XXX, XXX−XXX

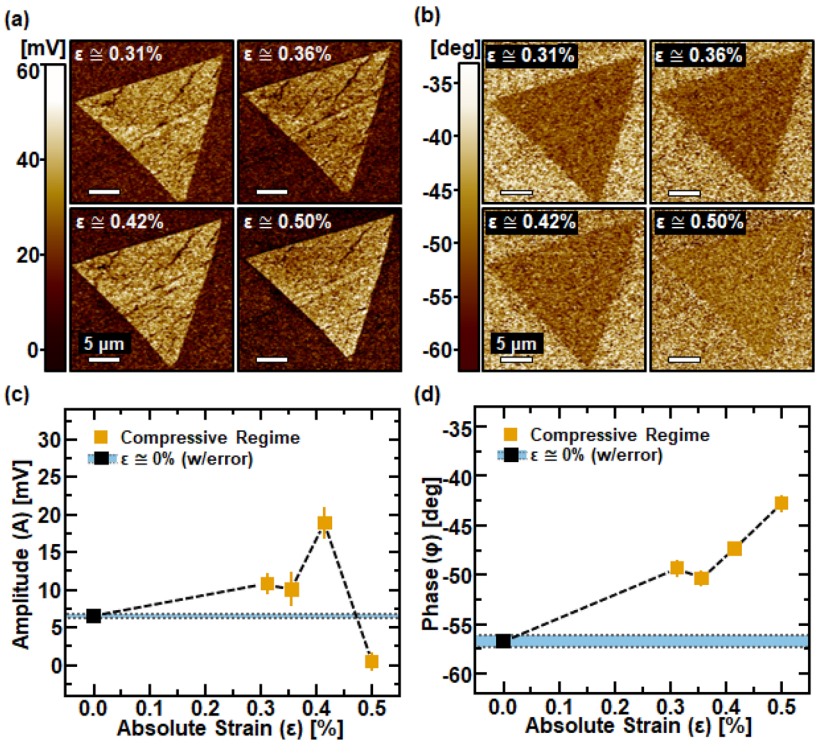

Figure 2. Compressive strain-correlated PFM characterization of ZnO NS. (a) Amplitude and (b) PFM phase images of a ZnO NS obtained under four different compressive strain conditions. (c, d) Strain-related PFM amplitude (c) and phase (d) responses obtained using the image intensities extracted from selected small scan regions on the ZnO-NS surface. The shaded region represents the unstrained result.

contact reached a normal loading force of 50 nN (see Supplemental Note S1). To induce an inverse piezoelectric response, an AC driving voltage $V_C = V_0 \cos(\omega t + \varphi)$ of 2 V_{AC} was applied to the tip−sample interface, generating a local electric field between the Au-coated PI and conductive cantilever-tip (Figure 1a). Deviations from the amplitude and phase components of the driving voltage feedback loop were subsequently collected using an external lock-in amplifier (LiA) and correlated to the inverse piezoresponse via 2D PFM image formation. Here, the measured amplitude (ΔA) and phase ($\Delta\varphi$) deviations represent the bias-induced electromechanical deformation and relative dipole polarization, respectively.[28] For an out-of-plane piezoresponse, this corresponds to vertical amplitude deflections of the cantilever and phase deviations of ±180°. Alternatively, lateral/torsional displacement of the cantilever along with phase deviations of ±90° will reflect in-plane piezoresponse. In Figure 1d, a typical PFM amplitude image taken over a large scan area (25 × 25 μm^2) illustrates the out-of-plane amplitude response of a ZnO-NS in the unstrained condition ($\varepsilon \sim 0.0\%$). Similarly, the small scan areas (1.5 × 1.5 μm^2) selected by regions 1−4 on the ZnO-NS surface in Figure 1d exhibited a noticeable amplitude response (Figure 1e).

Image analysis was used to examine the PFM amplitude images via the amplitude intensity histograms shown in Figure 1f and g. Amplitude intensity distributions were obtained from vertical deflection of the cantilever-tip as a set of voltage intensities (mV) measured by the AFM position sensitive photodiode (PSPD). The amplitude distributions represent the out-of-plane inverse piezoresponse of the ZnO-NS (black curve with blue curve fitting), tip interactions with the sample substrate (purple curve), and the mean background noise (orange curve) of the image, which was collected by performing a separate offset scan. The offset scan was obtained by raising the AFM probe far (~500 μm) above the sample surface to minimize the electrostatic contributions from the sample substrate and was taken following the completion of each strain-correlated PFM scan (detailed in Supplemental Note S2). Using a Gaussian fitting (e.g., blue curve and shaded region of the ZnO-NS amplitude), the mean intensity of each histogram distribution was extracted and used to quantify the strain-correlated inverse piezoresponse.

When comparing the extracted means of the ZnO-NS response taken from the large and small scan area image sets, we found that the amplitude intensity could vary significantly across strain configurations (see Supplemental Note S3). Notably, variations in the large scan area images showed several well-known tip−sample interactions, which may contribute to an overall enhancement of the measured ZnO-NS amplitude response. It was likely that a combination of short- and long-range electrostatics (ES) from the cantilever probe (i.e., tip ES, body ES), surface adhesion, and shifts in the contact resonance (CR) behavior of the AFM probe as it transitioned between the nonuniform elastic domains of the PI substrate and ZnO-NS surfaces, could elevate the final amplitude intensities in the PFM images.[29−31] Although PFM measurements in this study were performed well under the first CR frequency of the PFM probe, dynamics at the tip−sample interface, spatial variation in the sample modulus, and surface topography have been shown to contribute to pixel variation in the measured piezoresponse, leading to the large amplitude peak difference in Figure 1f.[32] Therefore, to minimize the substrate contributions, four small scan regions selected from the ZnO-NS surface (Figure 1e) without an exposed substrate were chosen for further analysis. Additionally, by reducing the measurement scan area, we could mitigate

https://doi.org/10.1021/acs.nanolett.3c01728
Nano Lett. XXXX, XXX, XXX−XXX

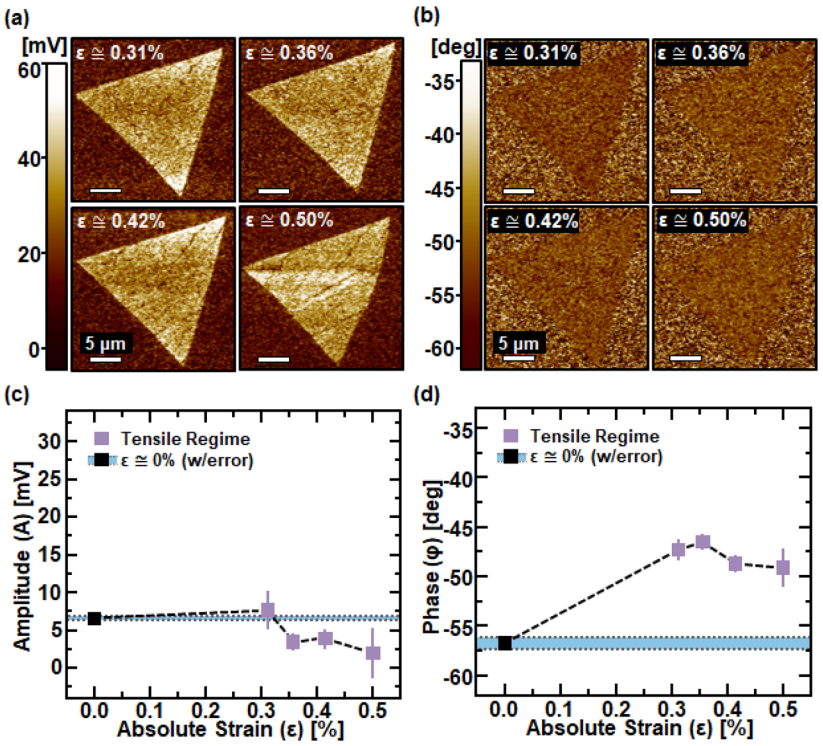

Figure 3. Tensile strain-correlated PFM characterization of ZnO NS. (a) Amplitude and (b) PFM phase images of a ZnO NS obtained under four different tensile strain conditions. (c, d) Strain-related PFM amplitude (c) and phase (d) responses obtained using the image intensities extracted from selected small scan regions on the ZnO-NS surface. The shaded region represents the unstrained result.

the influence of tip- and body-ES as the cantilever width (~25 μm) would remain invariant over the entire small scan area, and ES influence could be considered constant.

We used absolute strain percent values for comparison of compressive- and tensile-strain-correlated PFM characterization. Calculation of the absolute strain applied to the ZnO-NS was related via thickness of the PI substrate (t = 0.125 mm) and the radius of curvature (ROC) of the 3D printed mount with the following equation:

$$\left|\varepsilon = \frac{\tau}{ROC + \tau}\right| \times 100 \quad (1)$$

where τ is the half-thickness ($t/2$) of the PI substrate. Due to the very small thicknesses of the Ti/Au (5 nm/45 nm) layer and ZnO-NS (~2.4 nm), their influence on the calculated strain was not considered.

Figure 2 shows the amplitude and phase results of a single ZnO-NS measured under a series of compressive strains from 0.31% to 0.50%. From Figure 2a, the ZnO-NS amplitude response exhibited a strong output in the large scan area images for all strain configurations, suggesting that the propensity for out-of-plane inverse piezoelectric output is not suppressed under a static uniaxial in-plane compressive strain. The small dark striping across the surface of the ZnO-NS could be attributed to imperfections on the PI substrate. Likewise, the large scan area phase images in Figure 2b demonstrated a uniform response from ZnO-NS at different compressive strains. However, the apparent phase response gradually diminished as the compressive strain increased, which could be a result of reduced out-of-plane dipole polarization. From these large scan images, we could qualitatively observe the inverse piezoelectric response of the entire ZnO-NS, but these images were not sufficient to provide quantitative relationships.

To quantify the strain-related inverse piezoresponse, the mean intensity values were extracted from the four small scan regions selected from the ZnO-NS surface under each strain condition (outlined in Supplemental Note S3). The mean amplitudes were plotted as a function of absolute strain ($|\varepsilon\%|$) in Figure 2c and compared to the unstrained condition ($|\varepsilon\%| \sim$ 0.0%). In the unstrained condition, the measured PFM amplitude was ~6.6 mV, where the shaded dashed region represented the error (±0.3 mV) related to the zero-strain condition. As the compressive strain increased, mean PFM amplitude values (averaged from the four small scan areas) exhibited a noticeable increase above the unstrained condition, which peaked at ~18.9 ± 2.2 mV at $|\varepsilon\%| \sim$ 0.42%. Here, all of the measured amplitude values were well outside of the experimental error of the unstrained amplitude response, indicating the application of in-plane strain to be responsible for property variation. Additionally, a subsequent drop at the largest compressive strain of 0.50% was also observed, which could not be explained by amplitude analysis alone.

Upon PFM phase analysis, a more regular and monotonic increase was observed from the mean phase response in correlation with increasing compressive strain (Figure 2d). The mean value of phase response at ~0.0% strain was −56.8° ± 0.56°, where a maximum of −42.8° ± 0.53° was observed at 0.50%, giving a difference of ~14°. The more regular phase-strain relationship could be attributed to the reduced out-of-plane dipole displacement, which can be revealed qualitatively by the lowered contrast in the large scan area phase image (Figure 2b) at 0.50%. This observation suggested that the in-plane compressive strain may increase the out-of-plane piezoelectric response, until a threshold compressive strain subsequently limits out-of-plane amplitude and diploe displacement. The origin of this possible threshold may arise from so-

https://doi.org/10.1021/acs.nanolett.3c01728
Nano Lett. XXXX, XXX, XXX−XXX

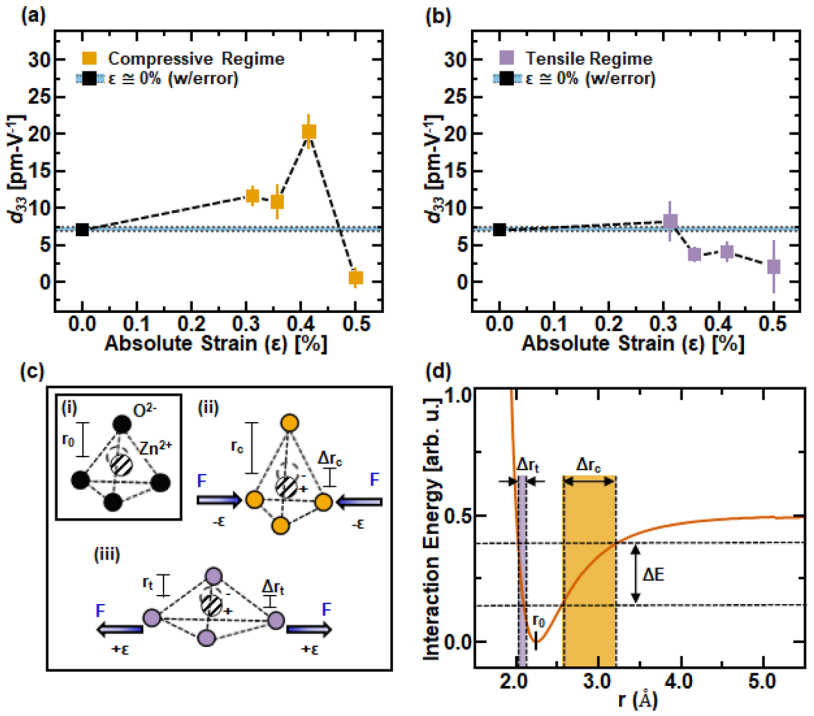

Figure 4. Strain-correlated piezoelectric property. (a) The out-of-plane piezoelectric coefficients (d_{33}) of ZnO-NSs under uniaxial in-plane compressive strain, showing an overall enhancement as the strain amplitude increases. (b) d_{33} of ZnO-NSs under uniaxial in-plane tensile strain, showing a general decrease trend beyond the unstrained case. (c) Schematic structure of tetrahedrally coordinated Zn^{2+} and O^{2-} ions in wurtzite ZnO (i), showing the distortion of the tetrahedron under compressive (ii) and tensile (iii) strains, and how this may modulate the out-of-plane dipole strength. (d) Generic Lennard-Jones potential between cation and anion, where the shaded regions present the possible out-of-plane displacement (Δr_t, Δr_c) under an equivalent electric field (ΔE).

called buckling of the ZnO-NS from residual surface compression effects.[33]

The inverse piezoresponse−strain relationship was then examined under tensile conditions. Here, the ZnO-NS also exhibited a uniform amplitude and phase response, as illustrated by the large scan area PFM images shown in Figure 3a,b, respectively. Compared to the compressive conditions, the tensile strain induced a similar amplitude response in the large scan areas. However, phase imagery revealed a reduced polarization for increased strain, indicated by the lowered phase contrast of ZnO-NS under tensile strains beyond ∼0.31%. The quantitative relationships in the tensile regime were extracted from small scan area images and plotted as functions of strain (Figure 3c,d). Compared to the compressive regime, the tensile strain yielded narrow change in both amplitude and phase response. All of the measured amplitudes exhibited a value lower than the unstrained condition and decreased to the lowest amplitude value of 1.9 ± 3.4 mV at the largest tensile strain of ∼0.50% (Figure 3c). A larger deviation of extracted mean intensities was observed from the largest tensile configuration possibly due to a slight distortion of the PI substrate on the mount, which can be seen from the ∼0.50% large scan area amplitude image. Phase analysis of the tensile regime indicated the mean phase responses were relatively invariant, with the extracted values occurring within a small range of −49.1° ± 1.1° to −46.5° ± 2.0°, approximately 7.6° to 10.2° from the unstrained condition, respectively. This suggested a weaker out-of-plane piezoelectric response when the NS was under tensile strain and dipole displacement was suppressed regardless of the degree to which tensile strains were applied. This was in sharp contrast to our observations regarding application of compressive strains and the corresponding notable variation of the inverse piezoresponse.

Finally, the piezoelectric coefficients (d_{33}) were quantified using mean amplitude intensities obtained from the small scan area images and cantilever AC-bias as

$$d_{33} = \delta \frac{\Delta A_z}{V_c} \tag{2}$$

where δ is the inverse optical lever sensitivity (InvOLS ∼ 10.7 ± 0.2 nm/V) calibration constant of the cantilever, and ΔA_z is the difference between the mean intensities of the PFM amplitude response and the averaged amplitude offset (∼10.3 ± 0.2 mV) (detailed in Supplemental Note S2).

Figure 4 shows the calculated d_{33} values in both the compressive (Figure 4a) and tensile strain (Figure 4b) regimes. Using the mean intensity value of the ZnO-NS amplitude response from small scan area images, the calculated d_{33} in the unstrained condition was ∼7.1 ± 0.32 pm V^{-1}, which was within the range of previously reported values of bulk ZnO crystals (8.8−12.4 pm V^{-1}).[14,22,34] Since d_{33} was calculated from the measured amplitude response, standard deviations represent variation between the measured amplitudes obtained in the four small scan regions. Compressive strain generally enhanced the d_{33} over the unstrained condition, reaching a maximum of ∼20.3 ± 2.3 pm V^{-1} at 0.42% strain and represented an ∼186% increase compared to the unstrained case. The large decline of d_{33} at ∼0.50% was directly associated with the amplitude response. As discussed above, this may indicate a threshold compressive strain in the setup for ZnO-NS.

https://doi.org/10.1021/acs.nanolett.3c01728
Nano Lett. XXXX, XXX, XXX−XXX

Alternatively, the tensile strains (Figure 4b) consistently lowered the d_{33} from the unstrained condition and reached a minimum of ~2.1 ± 3.6 pm V^{-1} at a tensile strain of 0.50%, which corresponded to an ~70% decrease from the unstrained case. Moreover, within the applicable strain range from compressive 0.42% to tensile 0.50%, the piezoelectric coefficient exhibited a substantial variation from ~20.3 to ~2.1 pm V^{-1}, corresponding to an order-of-magnitude change in the piezoelectric property. The substantial change in d_{33} values compared to the unstrained case and between different strain conditions suggested a large variation of the out-of-plane piezoelectric response could be possible when materials are subjected to in-plane strains. It is important to highlight that this effect is fundamentally different from either d_{31} or the flexoelectric effect. Although both effects depict the out-of-plane polarization induced by in-plane strain, they are an instantaneous effect and (if any) would induce transient polarization immediately following the strain being applied and then diminished via external/internal charge flow. However, this study investigated the effect from a static in-plane strain that is constantly applied to the material such that any transient contributions from other electromechanical coupling effects have been naturally balanced. Therefore, the measured out-of-plane piezoelectric responses only represent the targeted d_{33} effect under concurrent electric field excitation.

The strain-related piezoelectric property change could be attributed to the tetrahedrally coordinated structures of wurtzite ZnO.[35,36] For (0001)-oriented ZnO, when the lattice is deformed along the [0001] direction, the out-of-plane piezoelectric dipoles are created by the displacement (Δr_0) of Zn^{2+} ions from the center of the tetrahedrons of the O^{2-} as shown in Figure 4c-i (r_0 is defined as the equilibrium bonding length between Zn^{2+} and O^{2-}). When the lattice is subjected to an in-plane strain, deformation of the tetrahedrons could alter r_0, such that a different level of potential displacement between Zn^{2+} and O^{2-} ions along the vertical direction could be etsablished.[37] For example, under a lateral compressive strain, tetrahedra may deform into a slightly elongated geometry (Figure 4c-ii), leading to an increased Zn^{2+}-O^{2-} interatomic distance (r_c). Likewise, application of an in-plane tensile strain may slightly reduce the interatomic distance (r_t) (Figure 4c-iii). From the generic Lennard-Jones potential (LJP) plot shown in Figure 4d, the slope of the interatomic energy-displacement represents the propensity for out-of-plane ionic displacement. For a given energy input (ΔE, such as mechanical stress or external electric field), a larger interatomic distance (r_c) suggests that a larger ionic displacement (Δr_c) may be induced and subsequently a higher d_{33}. As the interatomic distance shifts to a smaller value (r_t) along the LJP profile, a larger energy-displacement slope indicates a smaller ionic displacement (Δr_t) may be achieved at the same ΔE, and thereby a lower d_{33}.

In summary, we quantified the out-of-plane piezoelectricity of 2D (0001)-oriented ZnO-NS, in correlation with in-plane strains, by using a strain-correlated PFM measurement. Analysis of the out-of-plane PFM phase response illustrated a propensity for dipole hindrance under in-plane tensile strain, while compressive strain facilitated higher out-of-plane dipole moment flexibility. This effect demonstrates that in-plane strains placed by bending can substantially influence the piezoelectric behavior of the (0001) surface-dominated ZnO-NSs. The maximum d_{33} was quantified at ~20.3 pm V^{-1} under a compressive strain of $|\varepsilon\%| \sim 0.42\%$, which was an ~186% increase when compared to ~7.1 pm V^{-1} in the unstrained configuration. Upon application of a maximum tensile strain of ~0.50%, the d_{33} was reduced to ~2.1 pm V^{-1} for an ~70% decrease from the unstrained case. Together, they presented a wide-range variation of d_{33} when the lattice was strained oppositely in-plane, which resulted in an order-of-magnitude change in the piezoelectric property. The observed out-of-plane piezoelectricity change could be attributed to interatomic Zn^{2+} and O^{2-} tetrahedron distortion that contributed to out-of-plane dipole modulation resulting from in-plane strain. This work experimentally revealed that uniaxial in-plane strain could substantially influence the out-of-plane piezoelectricity in the 2D piezoelectric lattices. This discovery suggests that in-plane strain, as an important and common factor, should be considered in the study and application of flexible piezoelectric materials, particularly when their thickness is small.

■ ASSOCIATED CONTENT

Data Availability Statement

The data sets generated and/or analyzed during the current study are available from the corresponding author upon reasonable request.

Supporting Information

The Supporting Information is available free of charge via the Internet at . Methods -3D Printed AFM Mounts, Sample Preparation; Section 1 (S1) - Piezoelectric characterization; Section 2 (S2) - Experimental parameters; Section 3 (S3) - Image Analysis The Supporting Information is available free of charge at https://pubs.acs.org/doi/10.1021/acs.nanolett.3c01728.

(PDF)

■ AUTHOR INFORMATION

Corresponding Author

Xudong Wang − *Department of Materials Science and Engineering, University of Wisconsin−Madison, Madison, Wisconsin 53706, United States;* orcid.org/0000-0002-9762-6792; Email: xudong.wang@wisc.edu

Authors

Corey Carlos − *Department of Materials Science and Engineering, University of Wisconsin−Madison, Madison, Wisconsin 53706, United States;* orcid.org/0000-0002-9398-2554

Jun Li − *Department of Materials Science and Engineering, University of Wisconsin−Madison, Madison, Wisconsin 53706, United States;* orcid.org/0000-0002-7498-6736

Ziyi Zhang − *Department of Materials Science and Engineering, University of Wisconsin−Madison, Madison, Wisconsin 53706, United States;* orcid.org/0000-0001-9102-8292

Kevin Jordan Berg − *Department of Materials Science and Engineering, University of Wisconsin−Madison, Madison, Wisconsin 53706, United States*

Yizhan Wang − *Department of Materials Science and Engineering, University of Wisconsin−Madison, Madison, Wisconsin 53706, United States*

Complete contact information is available at: https://pubs.acs.org/10.1021/acs.nanolett.3c01728

Notes

The authors declare no competing financial interest.

https://doi.org/10.1021/acs.nanolett.3c01728
Nano Lett. XXXX, XXX, XXX−XXX

■ ACKNOWLEDGMENTS

This work is supported by the National Science Foundation DMR-2114931 and the National Heart, Lung, and Blood Institute of the National Institutes of Health under Award Number R01HL157077. The content is solely the responsibility of the authors and does not necessarily represent the official views of the National Institutes of Health. C. Carlos thanks the support of the Graduate Engineering Research Scholars (GERS) funded by the Advanced Opportunity Fellowship (AOF), through the support of the State of Wisconsin and University of Wisconsin Graduate School.

■ REFERENCES

(1) Qi, J.; Lan, Y. W.; Stieg, A. Z.; Chen, J. H.; Zhong, Y. L.; Li, L. J.; Chen, C. D.; Zhang, Y.; Wang, K. L. Piezoelectric Effect in Chemical Vapour Deposition-Grown Atomic-Monolayer Triangular Molybdenum Disulfide Piezotronics. *Nat. Commun.* **2015**, *6* (1), 1−8.
(2) Johari, P.; Shenoy, V. B. Tuning the Electronic Properties of Semiconducting Transition Metal Dichalcogenides by Applying Mechanical Strains. *ACS Nano* **2012**, *6* (6), 5449−5456.
(3) Li, Z.; Lv, Y.; Ren, L.; Li, J.; Kong, L.; Zeng, Y.; Tao, Q.; Wu, R.; Ma, H.; Zhao, B.; Wang, D.; Dang, W.; Chen, K.; Liao, L.; Duan, X.; Duan, X.; Liu, Y. Efficient Strain Modulation of 2D Materials via Polymer Encapsulation. *Nat. Commun.* **2020**, *11* (1), 1−8.
(4) Ryu, Y. K.; Carrascoso, F.; López-Nebreda, R.; Agraït, N.; Frisenda, R.; Castellanos-Gomez, A. Microheater Actuators as a Versatile Platform for Strain Engineering in 2D Materials. *Nano Lett.* **2020**, *20* (7), 5339−5345.
(5) Li, J.; Kang, L.; Yu, Y.; Long, Y.; Jeffery, J. J.; Cai, W.; Wang, X. Study of Long-Term Biocompatibility and Bio-Safety of Implantable Nanogenerators. *Nano Energy* **2018**, *51* (May), 728−735.
(6) Zhang, Z.; Yao, C.; Yu, Y.; Hong, Z.; Zhi, M.; Wang, X. Mesoporous Piezoelectric Polymer Composite Films with Tunable Mechanical Modulus for Harvesting Energy from Liquid Pressure Fluctuation. *Adv. Funct. Mater.* **2016**, *26* (37), 6760−6765.
(7) Wang, X. Piezoelectric Nanogenerators-Harvesting Ambient Mechanical Energy at the Nanometer Scale. *Nano Energy.* **2012**, *1*, 13−24.
(8) Castellanos-Gomez, A.; Poot, M.; Steele, G. A.; Van Der Zant, H. S. J.; Agraït, N.; Rubio-Bollinger, G. Elastic Properties of Freely Suspended MoS2 Nanosheets. *Adv. Mater.* **2012**, *24* (6), 772−775.
(9) Lee, J.; Yun, S. J.; Seo, C.; Cho, K.; Kim, T. S.; An, G. H.; Kang, K.; Lee, H. S.; Kim, J. Switchable, Tunable, and Directable Exciton Funneling in Periodically Wrinkled WS2. *Nano Lett.* **2021**, *21* (1), 43−50.
(10) Akinwande, D.; Petrone, N.; Hone, J. Two-Dimensional Flexible Nanoelectronics. *Nat. Commun.* **2014**, *5*, 1−12.
(11) Wang, Z. L.; Wu, W. Piezotronics and Piezo-Phototronics: Fundamentals and Applications. *Natl. Sci. Rev.* **2014**, *1*, 62−90.
(12) Peng, Y.; Que, M.; Tao, J.; Wang, X.; Lu, J.; Hu, G.; Wan, B.; Xu, Q.; Pan, C. Progress in Piezotronic and Piezo-Phototronic Effect of 2D Materials. *2D Materials.* **2018**, *5*, 042003.
(13) Scrymgeour, D. a; Hsu, J. W. P. Correlated Piezoelectric and Electrical Properties in Individual ZnO Nanorods. *Nano Lett.* **2008**, *8* (8), 2204−2209.
(14) Zhao, M. H.; Wang, Z. L.; Mao, S. X. Piezoelectric Characterization Individual Zinc Oxide Nanobelt Probed by Piezoresponse Force Microscope. *Nano Lett.* **2004**, *4* (4), 587−590.
(15) Wang, Z. L.; Song, J. Piezoelectric Nanogenerators Based on Zinc Oxide Nanowire Arrays. *Science (80-.).* **2006**, *312* (5771), 242−246.
(16) Liu, S.; Wang, L.; Feng, X.; Wang, Z.; Xu, Q.; Bai, S.; Qin, Y.; Wang, Z. L. Ultrasensitive 2D ZnO Piezotronic Transistor Array for High Resolution Tactile Imaging. *Adv. Mater.* **2017**, *29* (16), 1606346.
(17) Wang, L.; Liu, S.; Zhang, Z.; Feng, X.; Zhu, L.; Guo, H.; Ding, W.; Chen, L.; Qin, Y.; Wang, Z. L. 2D Piezotronics in Atomically Thin Zinc Oxide Sheets: Interfacing Gating and Channel Width Gating. *Nano Energy* **2019**, *60* (March), 724−733.
(18) Lozano, H.; Catalan, G.; Esteve, J.; Domingo, N.; Murillo, G. Non-Linear Nanoscale Piezoresponse of Single ZnO Nanowires Affected by Piezotronic Effect. *Nanotechnology* **2021**, *32*, 025202.
(19) Wang, F.; Seo, J.-H.; Luo, G.; Starr, M. B.; Li, Z.; Geng, D.; Yin, X.; Wang, S.; Fraser, D. G.; Morgan, D.; Ma, Z.; Wang, X. Nanometre-Thick Single-Crystalline Nanosheets Grown at the Water-Air Interface. *Nat. Commun.* **2016**, *7*, 10444.
(20) Wang, F.; Yin, X.; Wang, X. Morphological Control in the Adaptive Ionic Layer Epitaxy of ZnO Nanosheets. *Extrem. Mech. Lett.* **2016**, *7*, 64−70.
(21) Yin, X.; Shi, Y.; Wei, Y.; Joo, Y.; Gopalan, P.; Szlufarska, I.; Wang, X. Unit Cell Level Thickness Control of Single-Crystalline Zinc Oxide Nanosheets Enabled by Electrical Double-Layer Confinement. *Langmuir* **2017**, *33* (31), 7708−7714.
(22) Carlos, C.; Wang, Y.; Wang, J.; Li, J.; Wang, X. Thickness-Dependent Piezoelectric Property from Quasi-Two-Dimensional Zinc Oxide Nanosheets with Unit Cell Resolution. *Research* **2021**, 1519340.
(23) Zhang, Z.; Carlos, C.; Wang, Y.; Dong, Y.; Yin, X.; German, L.; Berg, K. J.; Bu, W.; Wang, X. Nucleation Kinetics and Structure Evolution of Quasi-Two-Dimensional ZnO at the Air-Water Interface: An in Situ Time-Resolved Grazing Incidence X-Ray Scattering Study. *Nano Lett.* **2022**, *22* (7), 3040−3046.
(24) Megusar, J. Low Temperature Fast-Neutron and Gamma Irradiation of Kapton ® Polyimide Films. *J. Nucl. Mater.* **1997**, *245* (2−3), 185−190.
(25) Momma, K.; Izumi, F. VESTA 3 for Three-Dimensional Visualization of Crystal, Volumetric and Morphology Data. *J. Appl. Crystallogr.* **2011**, *44* (6), 1272−1276.
(26) Serles, P.; Arif, T.; Puthirath, A. B.; Yadav, S.; Wang, G.; Cui, T.; Balan, A. P.; Yadav, T. P.; Thibeorchews, P.; Chakingal, N.; et al. Friction of Magnetene, a Non-van Der Waals 2D Material. *Sci. Adv.* **2021**, *7* (47), 2041.
(27) Gnecco, E.; Bennewitz, R.; Socoliuc, A.; Meyer, E. Friction and Wear on the Atomic Scale. *Wear* **2003**, *254* (9), 859−862.
(28) Neumayer, S. M.; Saremi, S.; Martin, L. W.; Collins, L.; Tselev, A.; Jesse, S.; Kalinin, S. V.; Balke, N. Piezoresponse Amplitude and Phase Quantified for Electromechanical Characterization. *J. Appl. Phys.* **2020**, *128* (17), 171105.
(29) Robins, L. H.; Brubaker, M. D.; Tung, R. C.; Killgore, J. P. Isomorphic Contact Resonance Force Microscopy and Piezoresponse Force Microscopy of an Aln Thin Film: Demonstration of a New Contact Resonance Technique. *Nano Futures* **2020**, *4* (2), 025003.
(30) Wang, J. H. Substrate Effects on Piezoresponse Force Microscopy Electromechanical Responses of Piezoelectric Thin Films. *Int. J. Solids Struct.* **2017**, *128*, 149−159.
(31) Casper, C. B.; Ritchie, E. T.; Teitsworth, T. S.; Kabos, P.; Cahoon, J. F.; Berweger, S.; Atkin, J. M. Electrostatic Tip Effects in Scanning Probe Microscopy of Nanostructures. *Nanotechnology* **2021**, *32* (19), 195710.
(32) Killgore, J. P.; Deolia, A.; Robins, L.; Murray, T. W. Experimental Reconstruction of the Contact Resonance Shape Factor for Quantification and Amplification of Bias-Induced Strain in Atomic Force Microscopy. *Appl. Phys. Lett.* **2019**, *114* (13), 133108.
(33) Zhang, J.; Wang, C.; Adhikari, S. Surface Effect on the Buckling of Piezoelectric Nanofilms. *J. Phys. D. Appl. Phys.* **2012**, *45* (28), 285301.
(34) Christman, J. A.; Woolcott, R. R.; Kingon, A. I.; Nemanich, R. J. Piezoelectric Measurements with Atomic Force Microscopy. *Appl. Phys. Lett.* **1998**, *73* (26), 3851−3853.
(35) Lee, J. H.; Lee, W. J.; Lee, S. H.; Kim, S. M.; Kim, S.; Jang, H. M. Atomic-Scale Origin of Piezoelectricity in Wurtzite ZnO. *Phys. Chem. Chem. Phys.* **2015**, *17* (12), 7857−7863.
(36) Hill, N. A.; Waghmare, U. First-Principles Study of Strain-Electronic Interplay in ZnO: Stress and Temperature Dependence of the Piezoelectric Constants. *Phys. Rev. B - Condens. Matter Mater. Phys.* **2000**, *62* (13), 8802−8810.

https://doi.org/10.1021/acs.nanolett.3c01728
Nano Lett. XXXX, XXX, XXX−XXX

(37) Jung, Y. S.; Choi, H. J.; Park, J. W.; Cho, Y. S. Anisotropic In-Situ Stretching-Strain Engineering of Flexible Multilayer Thin-Film Nanogenerators with Cu Interlayers. *Nano Energy* **2021**, *82*, 105690.

https://doi.org/10.1021/acs.nanolett.3c01728
Nano Lett. XXXX, XXX, XXX−XXX